Quaternary Science Advances 2 (2020) 100010

Contents lists available at ScienceDirect

Quaternary Science Advances

journal homepage: www.journals.elsevier.com/quaternary-science-advances

The Idre marginal moraine – An anchorpoint for Middle and Late Weichselian ice sheet chronology

Johan Kleman [a,*], Martina Hättestrand [a], Ingmar Borgström [a], Frank Preusser [b], Derek Fabel [c]

[a] Department of Physical Geography, Stockholm University, 106 91 Stockholm, Sweden
[b] Institute of Earth and Environmental Sciences, University of Freiburg, Alberstrasse 23b, 79104 Freiburg, Freiburg, Germany
[c] Scottish Universities Environmental Research Centre (SUERC), College of Science and Engineering, University of Glasgow, East Kilbride, United Kingdom

ARTICLE INFO

Keywords:
Scandinavian ice sheet
Luminescence dating
^{10}Be dating
Interstadial
Idre moraine

ABSTRACT

We here report the results of luminescence and cosmogenic exposure dating of the Idre marginal moraine, located in the southern Scandinavian Mountains. This particular moraine is targeted because it is morphologically distinct and marks the margin of a former ice sheet. The till in the moraine contains erratics that provide strong evidence of flow from an ice sheet centred over Norway. The area immediately outside the moraine margin is an older residual soil. Luminescence ages of three samples taken from a sand lense within the moraine indicate that it formed at around 55 ka, during the early warm part of Marine Isotope Stage (MIS) 3. Median exposure ages (^{10}Be) of ten samples from boulders embedded in the surface till indicate that about 30 ka of ice-free time have elapsed since formation of the moraine. The difference between the age of the ridge and the duration of exposure provides a measure of the time of ice-cover in the ice sheet core area. Previous research indicates that final deglaciation of the site occurred at approximately 10 ka ago, which in combination with our results implies that the area around the Idre marginal moraine was ice free for ca. 20 ka, i.e. from around 55 ka to around 35 ka. Thereafter, the area was glaciated and the marginal moraine was covered by the Late Weichselian ice sheet for around 25 ka without experiencing any significant erosion or morphological destruction. While earlier studies have already pointed towards MIS 3 ice free conditions in northern and central Sweden, this study contributes a measurement-based duration estimate for the MIS 3 interstadial.

1. Introduction

For over a century, fresh-looking glacial landforms in the northern hemisphere were almost universally assigned to the last period of ice sheet cover (Mannerfelt, 1945; Aylsworth and Shilts, 1989), an assignment for which often no additional evidence beyond the morphological freshness was requested. It was assumed that older glacial landforms would typically be destroyed or severely eroded, and that older glacial events were only recorded in the stratigraphic and striae records. This paradigm about universal glacial erosion and non-survival of older small-scale forms was seriously challenged in the 1970′s and 1980′s (e.g Sugden and Watts, 1977; Lagerbäck and Robertsson, 1988). It is now widely recognised that areas with older preserved landforms can provide previously elusive information about pre-Last Glacial Maximum (LGM) conditions in formerly glaciated areas.

The mountains in west-central Sweden (Fig. 1) have a landform archive which is now considered to be an intricate mix of Late Weichselian deglaciation landforms, and residual and scattered landforms of older age (Lagerbäck and Robertsson, 1988; Borgström, 1989; Kleman and Borgström, 1990; Kleman, 1992).

In the 1980's and 1990's, intensive investigations of Quaternary stratigraphy and landform systems were conducted in northern Fennoscandia. Two separate Weichselian interstadials were identified both in north-eastern Sweden (Lagerbäck and Robertsson, 1988) and in central Sweden (Lundqvist and Miller, 1992). These interstadials were interpreted to correlate with the Brörup Interstadial (Marine Isotope stage (MIS) 5c), and the Odderade Interstadial (MIS 5a). At the time, it was generally accepted that large parts of Scandinavia were ice covered from MIS 4 (approximately 74 ka ago) until the last deglaciation at about 10 ka ago (i.e., Lagerbäck and Robertsson, 1988; Lagerbäck, 1988; Mangerud, 1991a,b). Later studies have challenged this view and a re-evaluation of dates in older studies (Wohlfarth, 2010) and new investigations show that large parts of Fennoscandia probably were ice free during parts of MIS 3 (e.g. Helmens et al., 2009; Hättestrand and Robertsson, 2010;

* Corresponding author.
E-mail address: Kleman@natgeo.su.se (J. Kleman).

https://doi.org/10.1016/j.qsa.2020.100010
Received 16 December 2019; Received in revised form 13 May 2020; Accepted 22 May 2020
Available online 27 May 2020

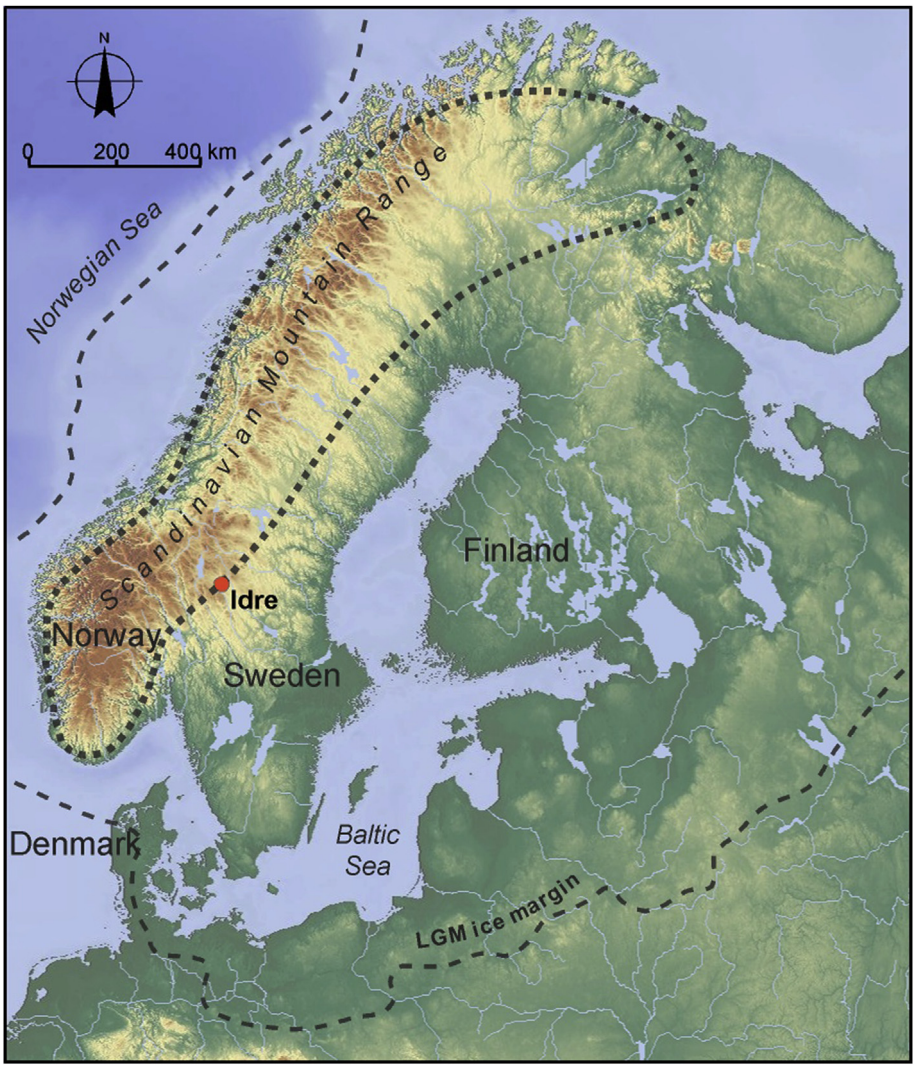

Fig. 1. Location map and ice sheet context. The figure shows two archetypical configurations of Scandinavian ice sheets (Kleman et al., 1997); limited and west-centred Scandinavian ice sheets over the mountain range during periods of moderate climatic deterioration, and full-grown Fennoscandian ice sheets during glacial maxima.

Ukkonen et al., 2011). However, the possible location and size of any remnant MIS 3 ice cap and the more precise chronology of ice-free conditions have warranted further investigation.

We here report dating results from the Idre marginal moraine (Fig. 2) which through its location has the potential to provide chronological constraints on the margin location of a limited pre-Late Weichselian ice sheet. We use luminescence dating of a sand layer within the moraine to calculate the time of formation, and cosmogenic dating of boulders embedded in the surface till of the moraine to constrain the duration of ice-free time since its formation. The difference between the two is a measure of the duration of ice-covered time in the ice sheet core area, the first of its kind. We have targeted this particular moraine because it is morphologically distinct and marks the edge of a till sheet in which erratics provide strong evidence of flow by a Norway-centred mountain ice sheet. In contrast to many local stratigraphic sequences, it can therefore with a fair degree of certainty be placed in a regional ice-sheet context (Fig. 1). Scandinavian ice sheets with their eastern margin at, or west of, Idre can be regarded as mountain-centred ice sheets (Kleman and Stroeven, 1997), and represent what Porter (1989) termed 'average glacial conditions'.

2. Regional setting

Städjan – Nipfjället is a mountain group reaching 1191 m a.s.l., surrounded by hilly plains and broad valleys with their elevations in the range of 600–750 m. The massif itself is geologically an outlier of the Caledonides (Fig. 3). The bedrock consists mainly of slates and mudstones with a number of sub-horizontal benches of very resistant quartzites. The overall relief features, with slopes between 15° and 40° and flat or gently sloping summit areas, is a common feature for all the surrounding mountain groups. Detached or surficial boulders on the uplands are almost exclusively of the local quartzite. Quartzite boulders are common on till surfaces as well as on the residuum surfaces. On till surfaces, both rooted boulders and boulders that appear loosely dropped on the surface are found. On the residuum surface composed of soft weathered and fragmented mudstone, all quartzite boulders are unrooted, also very large boulders are loosely deposited on the surface of the residuum.

The western segment of the investigated moraine ridge partially wraps around a low summit (1025 m a.s.l.) on the bedrock ridge connecting the Städjan and Nipfjället summits. The Idre moraine was originally mapped and classified as an esker (Mannerfelt, 1938). As we show,

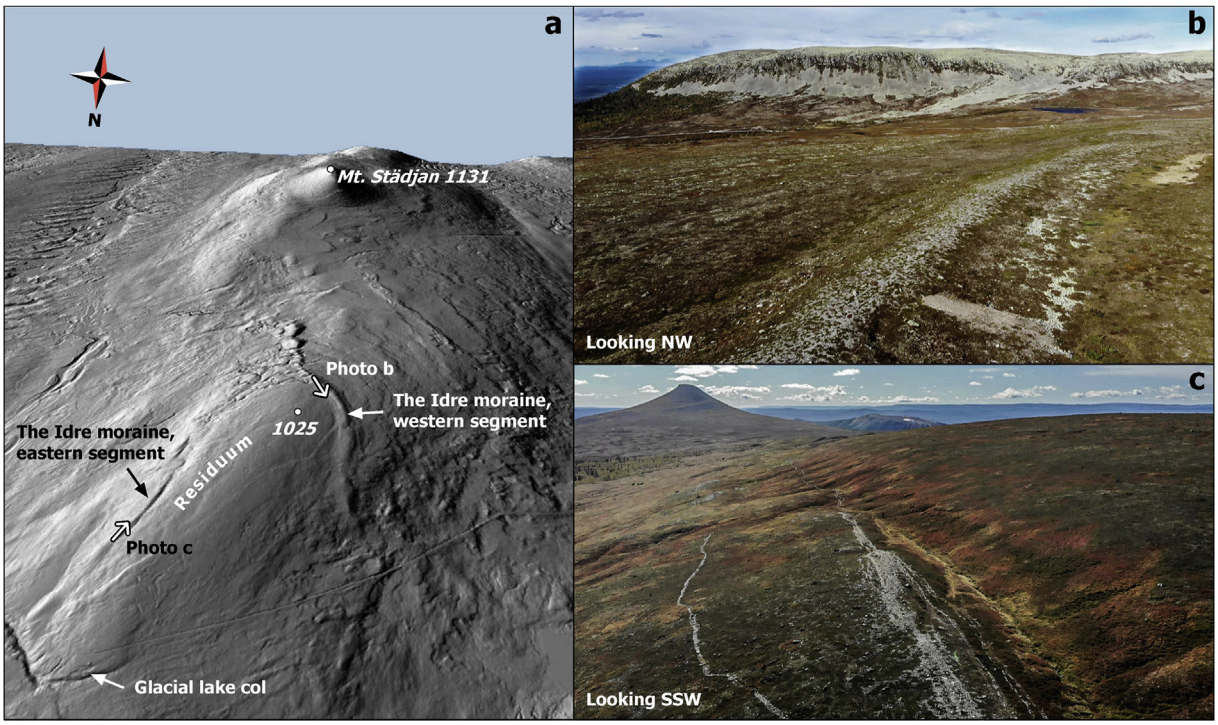

Fig. 2. The layout and topographical context of the Idre moraine. Photo directions for drone photographs 2b and 2c are indicated by arrows in Fig. 2a. In Fig. 2b, the location of the investigated section is indicated by the excavation scar in the foreground. In Fig. 2c, the crest line of the eastern part of the moraine is indicated by the broad whitish footpath. The hill on the right-hand side of the photograph is residuum-covered. The left-hand foreground is till-covered, with the eastern moraine segment marking the upper limit of till covered terrain. For scale: The distance between the two summits marked in (a) is 4.1 km.

this classification is erroneous, the ridge is almost entirely composed of till and simply a morphological expression at the edge of a till sheet impinging on the mountain. A shorter but morphologically similar moraine fragment wraps round the eastern side of the hill at a similar elevation. This segment, like the western one, also marks the upper limit of the till sheet. In the following we treat these two fragments as one unit, assuming that they represent the same glacial history. We first investigated this site in 1989, when a trench was machine-excavated through part of the western moraine segment. At the same time, a 3 m deep probing excavation was made at the 1025 m summit, confirming the absence of any till. The faint distal-sloping layering and the location of the moraine at the extreme edge of a till sheet resting on residual soil established its origin as a lateral/marginal moraine (see Figs. 4 and 5). In the initial excavation in 1989 we noted the presence of sand lenses sloping in the distal direction.

In the year 2000, an initial cosmogenic date on a boulder embedded in the till surface of the western moraine segment indicated that our working hypothesis that the formation of this ridge is unrelated to the last deglaciation may be correct. This date (NIP-10), is reported in the current data set. In 2015, we conducted partial excavation of the moraine ridge for luminescence-sampling, and new sampling of boulders for cosmogenic dating was conducted.

Dating control on the formation of the moraine can with relatively few assumptions be placed in a regional ice-sheet context. We assume that during a cooling phase, ice expanded out from the Norwegian mountains, and that flow from restricted ice sheets thus was from the westerly sector. We further assume that the moraine, which genetically is a marginal moraine, marks the edge of an ice sheet during a climatically governed marginal standstill. There are no indications that it could be a surge-related moraine and thus unrelated to climate.

The elevation of the moraine is within 400 m of the surrounding valleys and plains, indicating that the regional lowland ice-margin was close by, probably less than 10 km distant, when it was formed. The transport direction, as inferred from characteristic erratics, was from the northwest sector, showing that it formed at the eastern margin of a Norwegian mountain ice sheet. Mass-balance considerations support this conclusion. Topography rises to the west, and the present glaciation limit is strongly sloping in the same direction. Hence, only a small westerly located ice sheet can be expected to have its margin in climatic balance at Idre.

3. Methods

3.1. Sections and sampling

The original section in 1989 was dug perpendicular to the long axis of the western moraine segment, from the distal side towards the centre of the ridge. The excavated pit (coordinates 61°56′56.7"N, 12°50′50.7"E) reached a maximum depth of 4.3 m (Figs. 4 and 5) of which the upper meters were till, with pods of gravelly-stony material. Sub-horizontal and discontinuous sand lenses of 15–20 cm thickness occurred in the lower part of the section. The contact to weathered shale bedrock could be followed over 10 m in the original section (Figs. 4 and 6a). In August 2015, the section was re-excavated and the uppermost sand lens sampled for luminescence dating. The excavation was performed at the same spot as earlier, however, it continued about 1 m further in on all sides to ensure fresh section walls. This time the excavator was smaller and could only dig down to a depth of about 3 m and the mudstone bedrock was not reached. Logging was performed on a one meter wide part of the section perpendicular to the moraine long axis.

The upper part of the section was till (Figs. 6 and 7), as observed during previous field work. However, in the shallower 2015 section only one clear sand layer was visible in the lower part. The sand layer was present throughout the pit and was slightly tilted away from the moraine

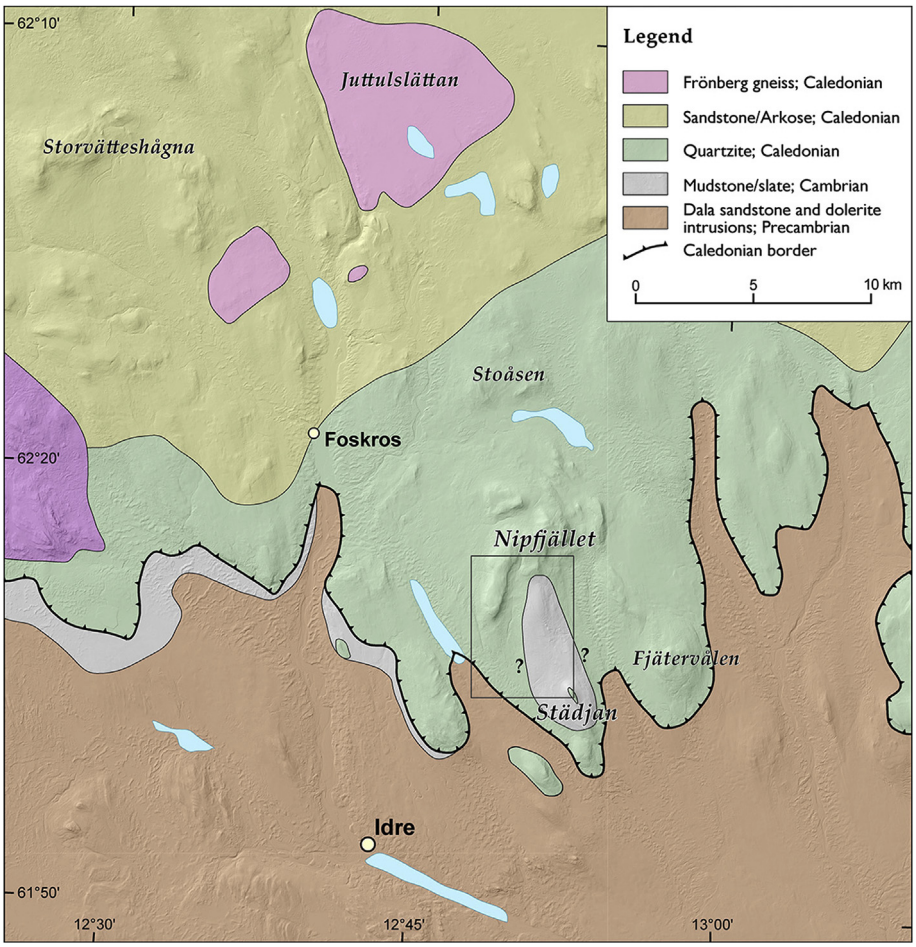

Fig. 3. Bedrock geology of the Idre area (simplified after Delin and Thelander, 2006). Question marks for uncertainties regarding the extent of mudstone/slate. The inset rectangle shows the outline of the geomorphological map in Fig. 11.

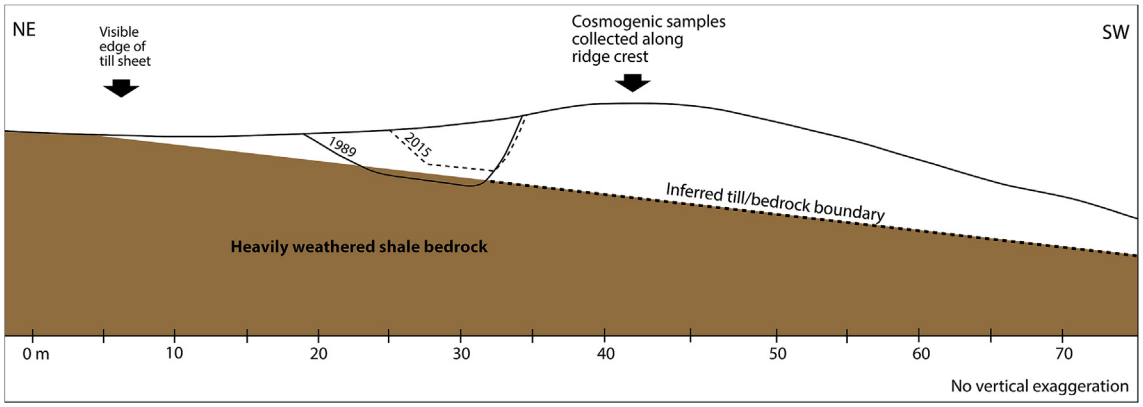

Fig. 4. Section across the western segment of the Idre moraine. The outlines of the 1989 and 2015 sections are shown. The 2015 section, which was sampled for luminescence dating, extended the previous section 1 m into the sidewalls of the section. No vertical exaggeration.

long axes towards the distal side of the ridge. The sand was well-sorted and slight grain size changes occurred as sub-horizontal bands in the layer. Field interpretation suggested that this could be outwash material deposited just outside the marginal moraine when it formed. We expected that the material therefore could have been well bleached before deposition. Successful luminescence dating of the sand would give the age of moraine formation since it would date material incorporated in the moraine during its formation. From the sandy layer, luminescence samples were taken by hammering opaque tubes into the freshly cleaned section wall, sealing them off and placing them in light-proof plastic bags. For all luminescence samples, material was also taken from the surrounding sediment for dose rate measurements.

Boulders for cosmogenic dating were sampled along 100 m lengths of the crests of the western and eastern moraine segments. The crest of the

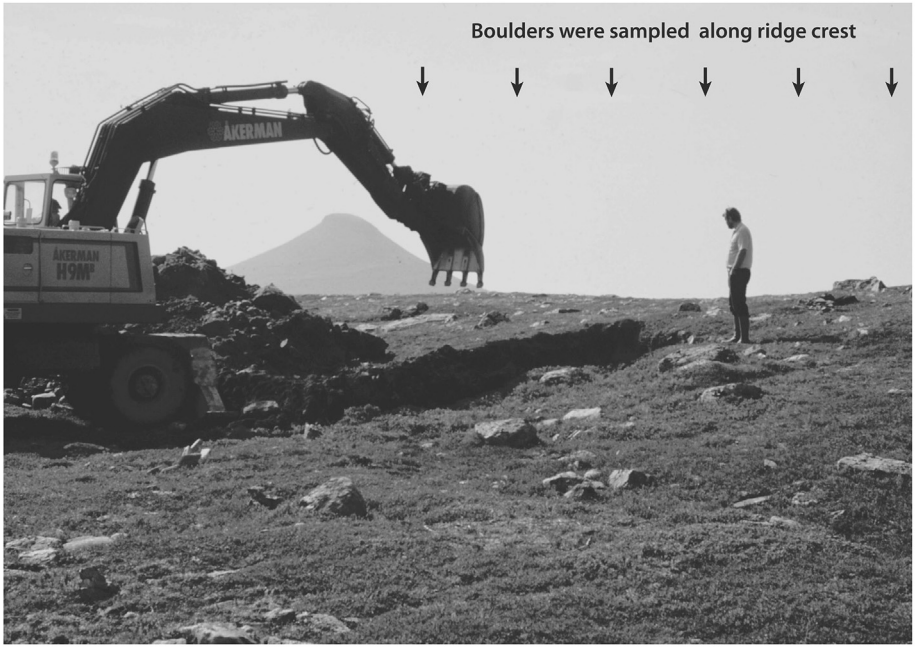

Fig. 5. The distal side of the western segment of the Idre moraine. The summit of Mt Städjan (1131 m a.s.l.) is visible in the background. Till thickness decreases from > 5m at the ridge crest to less than 0.5 m in the foreground of the photo. Seven cosmogenic samples were collected along 100 m of the single-crested ridge.

western segment is nearly flat over an 8–10 m width, and the along-ridge slope of the sampled section is less than 2°. The ground surface shows no indication of significant gravity induced processes. We sampled upper surfaces of boulders clearly rooted in the till (Fig. 8). All sampled boulders were of quartzite, which in the local bedrock occurs as 5–15 m thick benches, interspersed with the mechanically much weaker mudstone. The quartzite is widespread in the bedrock of the region. It outcrops in many places within a 2 km radius from the site and we are thus unable to make inferences about transport distances and pathways for the sampled boulders. Frönberg gneiss, outcropping 20–40 km distant in the sector between west and north, is a common but not major constituent of the till. It mostly occurs as small stones and pebbles. Its presence suggests that the moraine was formed by an ice sheet with its centre of mass northwest of Idre. The eastern ridge segment was less rich in boulders suitable for dating and only three boulders were sampled.

3.2. Geomorphological analysis

A geomorphological map was constructed by interpretation of two remotely sensed data sets; LIDAR data with 2 m resolution and colour infrared stereo photographs at a scale of 1:60,000. Field investigations in the Städjan – Nipfjället massif have been performed by team members since 1977, with a focus on genetic classification of landforms, and crosscutting and relative-age relationships. Morphological information pertinent to this study is found in Mannerfelt (1938, 1945), Kleman (1988), and Borgström (1989, 2017).

3.3. Luminescence dating

All laboratory work on the luminescence samples was done under subdued red-light conditions. Sand was retrieved from the inner part of the sampling tubes and the fraction 125–160 μm was extracted by wet sieving. Carbonates and organic matter were removed by 15% HCl and 30% H_2O_2. Quartz and K-feldspar grains were separated out using LST Fastfloat heavy liquid density separation at 2.70 and 2.58 g cm^{-3}, respectively. The quartz grains were etched for one hour in 40% HF, where after they were rinsed and immersed in 32% HCl for one hour to remove fluorides. Before measurement of a sample, sand grains were mounted on a surface area of about 1 mm on stainless steel discs, using silicon spray. Measurements were carried out using a Freiberg Instruments *Lexsyg Research* luminescence reader (Richter et al., 2013). Initial tests showed that the quartz samples had no luminescence signal so the following measurements were focused on the K-feldspar grains. For stimulation an 850 nm IR laser with the power set to 250 mW cm^{-2} was used. Detection was by an ET-9235QM photomuliplier and the detection filters used were Schott BG 39 (3 mm) and AHG BrightLine HC 414/46 nm interference filter (3.5 mm). Measurement of equivalent Dose (D_e), also sometimes referred to as palaeodose, was performed using the modified single aliquot regenerative dose (SAR) protocols (Murray and Wintle, 2000) presented in Table 1.

To test the luminescence characteristics of the studied sediments, measurements of residual dose, dose recovery and fading were performed. For the first two of these experiments, samples were first bleached with the in-build sun-light simulator for 3600 s. For the residual dose test, D_e of the samples was then measured using the SAR protocol given in Table 1 but adjusting the given dose to the expected level. We observe mean values ($n = 6$) of 4.37 ± 0.10 Gy (IRSL), 1.50 ± 0.08 Gy (IR-50/150), 2.29 ± 0.28 Gy (IR-50/225), 8.56 ± 0.07 Gy (pIR-150), and 25.72 ± 0.11 Gy (pIR-225). This indicates that strong bleaching for one hour reduces the IRSL signal to <3% (<5 Gy) of the natural level, whereas higher residuals of 6% (c. 9 Gy) for pIR-150, and of 17% (c. 25 Gy) for pIR-225 are observed. However, the implications for dating are not straight forward, as the bleaching conditions in the laboratory are not similar to those in nature. Nevertheless, it is clear that partial bleaching may have a much higher effect on the pIR signal compared to IRSL, as already pointed out by previous authors (e.g. Buylaert et al., 2012). For dose recovery, a dose in the range of the expected dose of the natural samples was applied. While for IRSL a recovery 94% is quite good, values of 91% for IR-50 from the pIR-protocols, and of 90% for pIR-150 are just within the accepted limits (Wintle and Murray, 2006). For pIR-225, a dose recovery of only 81% is considered critical. Interestingly, problems with this protocol have been reported mainly when applying low test dose, but we use a test dose of ca. 63 Gy, identical to the lowest irradiation step. Furthermore, only mild changes in sensitivity are observed

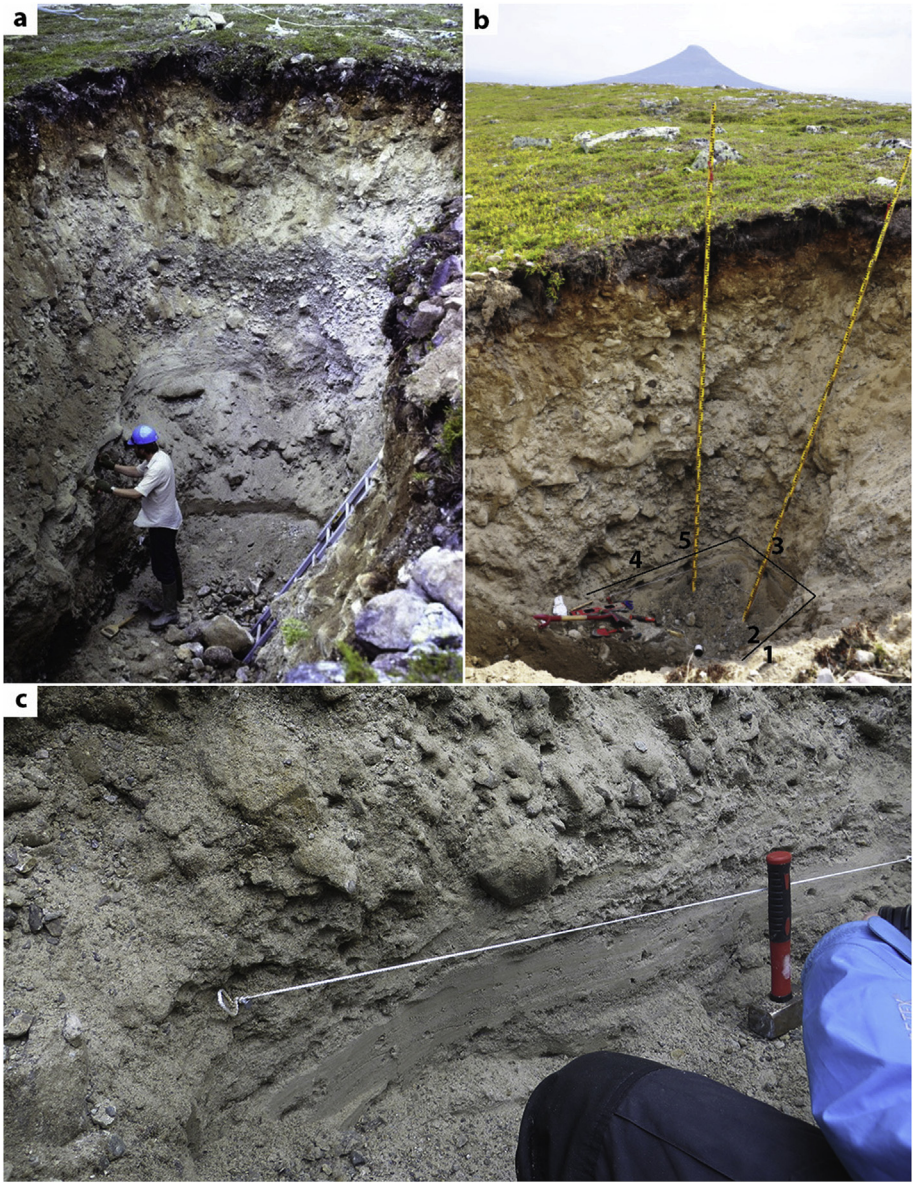

Fig. 6. a) The 1989 section reached a depth of 4.3 m and show several sand layers in the lower part of the section, and also the contact to weathered bedrock. b) the site was re-excavated in 2015. Compared to the 1989 section, the 2015 section was about 1.5 m less deep and extended 1 m into the sidewalls. In 2015, five luminescence samples were taken in the laminated sandy layer in the lower part of the section. The black line indicates the upper part of the sandy layer and the numbers show the position of the luminescence samples. After some initial test measurements sample 1, 2 and 3 were selected for further measurements and the calculated luminescence ages are based on these three samples. c) close-up of the sampled sandy layer. The white rope is horizontal and a reference for the tilt of the layer.

and these are present in all protocols (Fig. 9).

Fading tests follow Auclair et al. (2003) by monitoring signal loss in L_x/T_x measurements with different delay times between irradiation and optical stimulation (0, 100, 1000, and 10′000 s), each repeated three times (zero delay four times). For the three low temperature (IRSL, IR-50) measurements, we observe identical fading rates of 1.2 ± 0.2, 1.2 ± 0.9, and 1.3 ± 0.2 g/decade, and values of 0.2 ± 0.2 (pIR-150) and 0.4 ± 0.3 (pIR-225) g/decade for the measurements at elevated temperature. As storage tests appear to rather overestimate the real signal loess in nature (Wallinga et al., 2007; Reimann et al., 2011; Lowick et al., 2012), the potential effect on age calculation should be minor if not negligible.

For all samples we observe quite broad but none-skewed dose distributions, with occasional apparent outliers at the upper edge (Fig. 10). Overdispersion values are similar for all samples and approaches, with a mean of $22 \pm 3\%$. All observations in combination are interpreted to represent complete resetting of the luminescence signal prior to deposition. Hence, mean D_e was calculated using the Central Age Model (CAM) of Galbraith et al. (2007).

The concentration of dose rate relevant elements was determined by high-resolution gamma spectrometry (cf. Preusser and Kasper, 2001). An internal K-content of feldspar of $12.5 \pm 1.0\%$ was assumed (Huntley and Baril, 1997) and an a-value of 0.07 ± 0.02 was used. Cosmic dose rate was determined following Prescott and Hutton (1994). Dose rate calculation was done using ADELE software (Degering and Degering, 2020).

3.4. Cosmogenic dating

All rock samples were crushed and sieved to extract the 250–500 μm size fraction. Quartz was isolated by *aqua regia* leaching, feldspar floatation and magnetic separation. Quartz was then sequentially leached in 2% HF/1% HNO_3 to remove any remaining meteoric ^{10}Be. Be and Al isotope extraction chemistry was conducted at the Scottish Universities Environmental Research Center (SUERC) and at the Research School of Earth Sciences, Australian National University, following standard procedures (Kohl and Nishiizumi, 1992). After digestion in concentrated HF we removed an aliquot of the samples for ICP-OES analysis to determine the total Al and Be content of the sample. Samples were then dried down and Be and Al were isolated and purified via ion chromatography. After

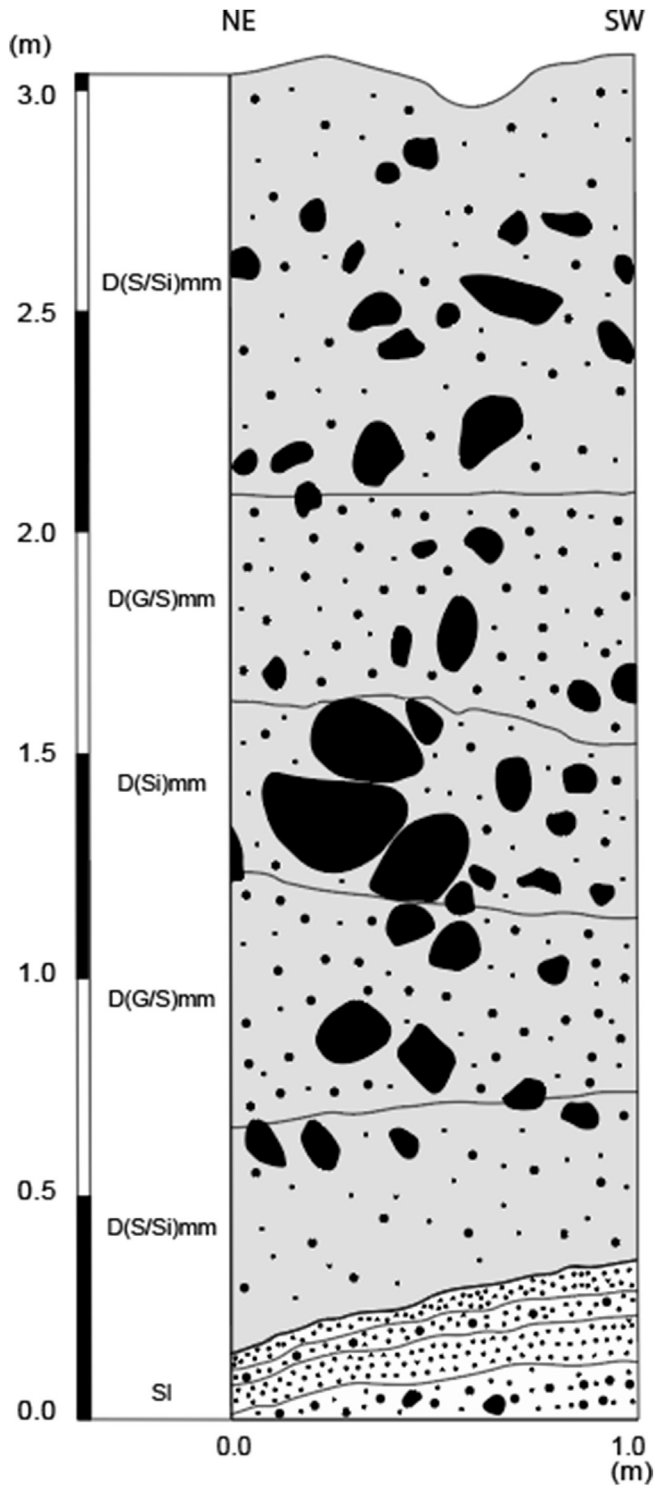

Fig. 7. Log of sediment units in the pit excavated in 2015. The log shows a 1 m wide part of the section on the SE wall of the pit. The SW part of the log is towards the proximal side of the moraine ridge and the NE part is towards the distal side. Grey represents diamicton and white represents sorted sandy/silty sediments. Facies codes: Dmm (diamicton, matrix-supported, massive) and Sl (Sand, laminated). Letters within brackets represent the dominant grain size in the matrix of the diamicton: G (gravel), S (sand), Si (silt).

oxidation, BeO was mixed with Nb-powder (ratio: 1:6) and Al_2O_3 was mixed with Ag-powder (ratio: 1:2) and then pressed into copper cathodes ready for AMS (accelerator mass spectrometry). Isotopic ratios were measured at ANSTO (Antares; n = 1) and at SUERC (n = 14). Be results were normalised to NIST SRM4325, with a ratio of $2.79{\cdot}10^{-11}$ (Nishiizumi et al., 2007). Al results were normalised to Purdue Z92-0222, with a ratio of $4.11{\cdot}10^{-11}$. For the ^{26}Al measurement, the total Al content determined by ICP-OES, was used to calculate the ^{26}Al concentration. Sample isotopic ratios were corrected for a procedural chemistry background of 61000 ± 11000 ^{10}Be atoms, except for NIP-12. This sample was processed in 2001 when we spiked with a larger ^{9}Be mass and measurement procedures were not as advanced as today. The procedural blank correction for this sample was 146000 ± 48000 ^{10}Be atoms, or 1.5% of the total ^{10}Be measured.

All exposure ages were calculated using version 2.3 of the online exposure age calculators formerly known as the CRONUS-Earth online exposure age calculators (Balco et al., 2008; http://hess.ess.washington.edu). We used the Lal/Stone time-independent scaling scheme (Lal, 1991; Stone, 2000) with a global calibration of the ^{10}Be spallation production rate of 4.00 ± 0.32 atom/g/a (Borchers et al., 2016) and a regional Scandinavian ^{10}Be spallation production rate of 4.28 ± 0.15 atom/g/a (Stroeven et al., 2016) downloaded from the ICE-D database (http://calibration.ice-d.org/). The ^{26}Al production rates are derived by multiplying the calibrated reference Be-10 production rate by the production ratio. Our apparent exposure ages are uncorrected for glacioisostatic uplift and snow-cover, which might lead to overestimation of the production rates and thus a slight underestimation among our reported ages. The effect of glacioisostatic adjustments is negligible compared to uncertainties associated with other factors such as temporal change in air pressure (Young et al., 2013) and long-term changes in snow depth are unknown.

4. Results

4.1. Morphological analysis

The investigated ridge is the highest and most distal of a series of marginal/lateral moraines at Städjan – Nipfjället (Figs. 2 and 11). The till sheet on the western slope of the Städjan – Nipfjället bedrock ridge ends at this moraine, which laps onto the weathering mantle that constitutes the summit area of the hill. The surface of the shallow depression between the moraine ridge and the weathering mantle of the bedrock ridge has abundant sorted polygons. These stop where the thickness of till drops below approximately 0.3 m, and larger stones no longer are present. Large sorted polygons on adjacent mountain groups have been demonstrated to be glacially overridden and being of an interstadial rather than Holocene origin (Kleman and Borgström, 1990). The excavated section confirms that the till thickness drops to less than 0.3 m towards the east, and surface observations indicate that till is entirely lacking towards the summit of the hill.

A conspicuous feature between Städjan and Nipfjället is the presence of large boulder masses which have been glacially dragged from the summit flat of Nipfjället and deposited in the shallow valley south of the source area. The transport direction and arrangement of the boulder masses exclude alternative mass-wasting explanations. They are inferred to be genetically similar to the features described on Mt. Fulufjället and other mountain groups in both the southern and northern parts of the mountain chain (Kleman and Borgström, 1990, 1994; Kleman, 1992). In most cases these boulder masses appear to be transported felsenmeer material and do not represent freshly eroded material.

Towards the north, the western moraine segment lowers slightly in elevation and continues as a series of disconnected mounds that form an arc into the shallow valley SE of Nipfjällets southern spur (Fig. 11c). The topographic context is such that it is likely that an ice-dammed lake formed there. A spillway at the col (Fig. 2) cut through approximately 3 m of till and residuum and into bedrock. A series of marginal meltwater channels of unknown age cut the western moraine segment at approximately 60° angle. If these are truly marginal, they outline a local ice margin that is not conformable with the moraine.

The crests of both segments of the moraine are studded with rooted

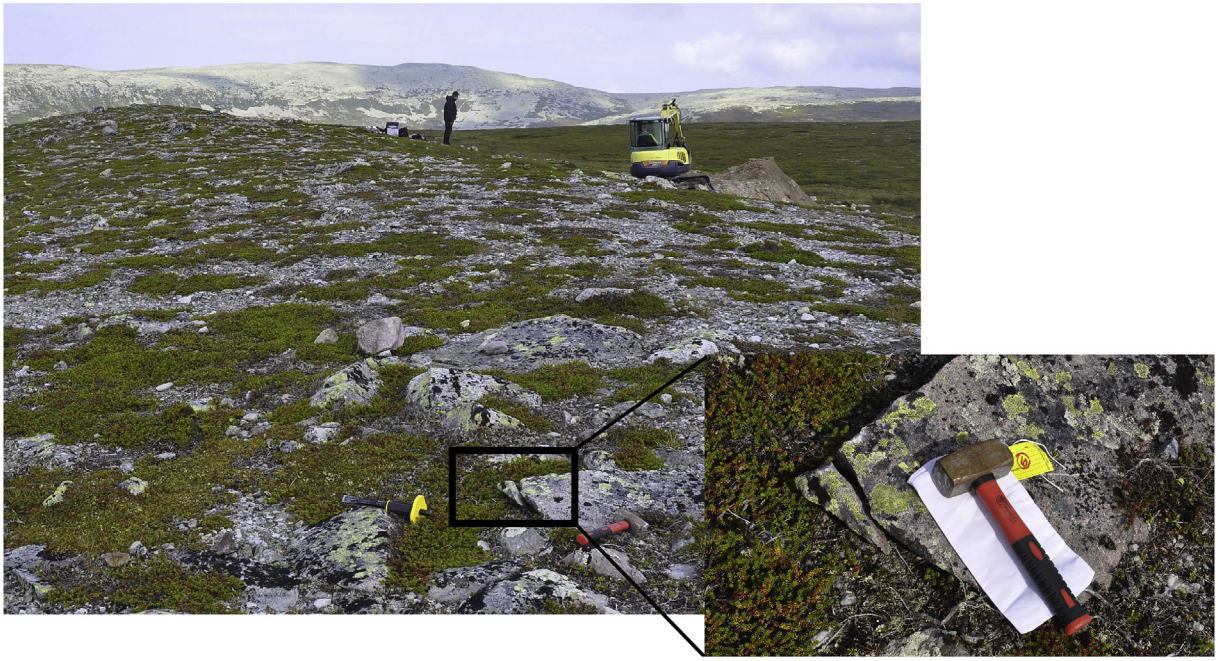

Fig. 8. The crest of the western moraine segment. The excavator and person indicate the location of the excavation pit. Part of the summit plateau of Mt Nipfjället in the background. Close-up of one of the sampled boulders. Corners and fractures of the very resistant quartzite in the boulders were exploited for sampling.

Table 1
Overview of the SAR protocols used in the present study.

Step	IRSL50	IRSL50-150/pIR150	IRSL50-225/pIR225
1	Preheat at 180 °C for 10s	Preheat at 180 °C for 10s	Preheat at 250 °C for 60s
2	IR stimulation at 50 °C for 150s	IR stimulation at 50 °C for 150s	IR stimulation at 50 °C for 150s
3	Test dose	IR stimulation at 150 °C for 200s	IR stimulation at 225 °C for 200s
4	Preheat at 160 °C for 10s	Test dose	Test dose
5	IR stimulation at 50 °C for 150s	Preheat at 160 °C for 10s	Preheat at 250 °C for 60s
6	Dose (to step 1)	IR stimulation at 50 °C for 150s	IR stimulation at 50 °C for 150s
7		IR stimulation at 150 °C for 200s	IR stimulation at 225 °C for 200s
8		Dose (to step 1)	Dose (to step 1)

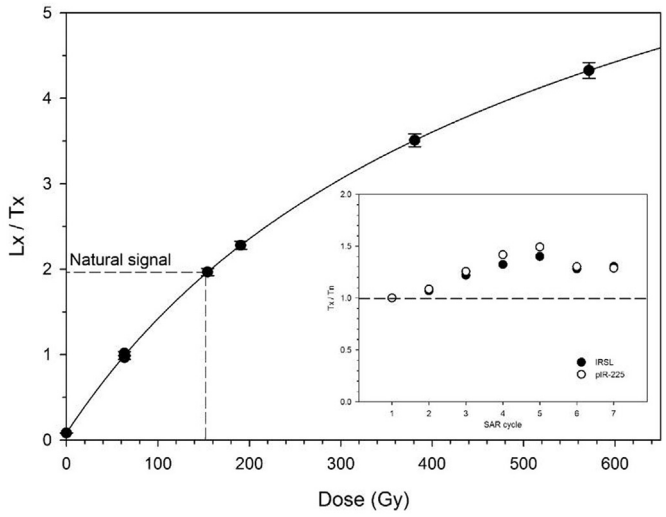

Fig. 9. Typical dose response curve indicating that the samples are far from saturation. Inset: The observed change in samples sensitivity is rather small and very similar for IRSL (measured at 50 °C) and pIR-225.

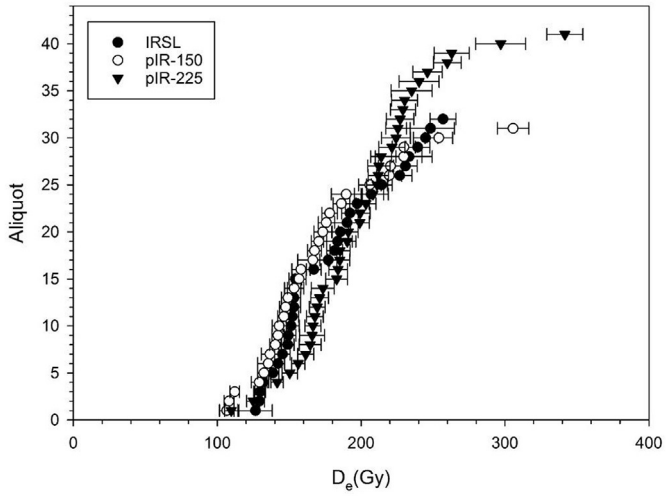

Fig. 10. Example De distributions plots reveal broad but Gaussian-shaped spread of data.

boulders, with the surface material between boulders being gravelly/stony, with sparse shrubs and herbs providing a stabilizing root mat (Fig. 8). There is no morphological indication that the moraine is a multi-generational feature. We infer that the sampled boulders were deposited as a normal constituent of the till during the final stages of moraine-building at the site. Cosmogenic dating of such boulders should therefore give a measure of the ice-free time elapsed since its formation. The morphological analysis indicates that the investigated western and the less prominent eastern moraine segment reflect a climatically governed standstill of the ice margin of a restricted ice sheet with its centre of mass over southern Norway. The similarity in morphology and elevation of the two segments is striking but the morphology where the two ridges are in close proximity on the SE slope of the 1025 m hill is unclear and their precise relationship therefore difficult to establish.

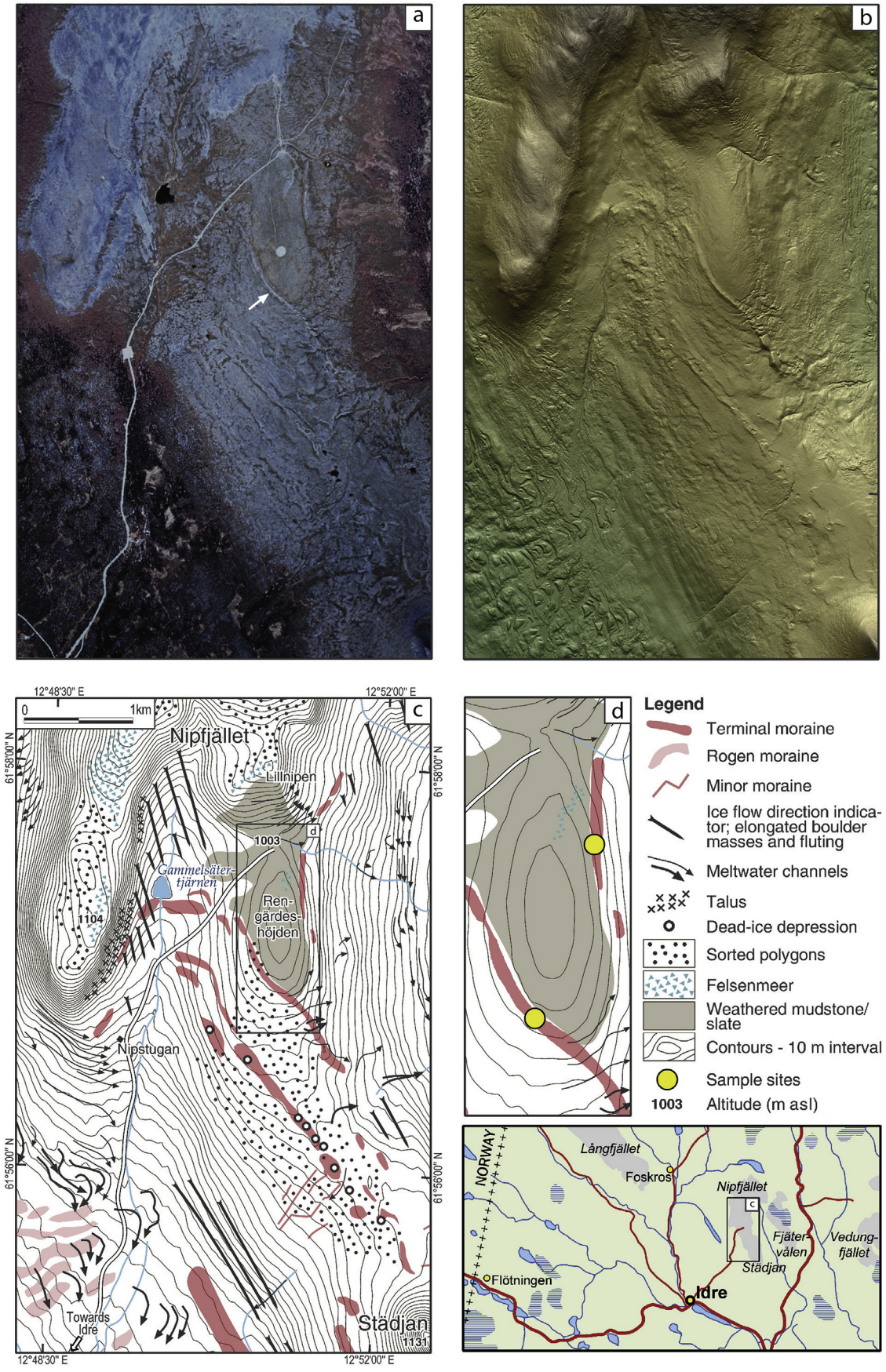

(caption on next page)

Fig. 11. a) Colour infrared photograph of the area between the Nipfjället and Städjan summits. Deep blue colour is mostly felsenmeer and rock outcrops, lighter blue is predominantly the regional till sheet. Weathered mudstone is more brownish than the till. The western (shown by arrow) and eastern segments of the Idre moraine wrap around the 1025 m hill between Nipfjället and Städjan. The white circle on the hill summit is a reindeer corral. b) Digital terrain model with a 2-m grid and a vertical resolution of 0.2 m. Artificial lighting is from the north. The western segment of the Idre moraine is the most prominent ridge near the centre of the image. Several subdued subhorizontal moraine systems are visible lower on the slope. c) Morphological map of the area. The core area of a weathering mantle exposed at the surface is shown in medium grey. The Idre moraine marks the uphill edge of the continuous till sheet. The excavation site (1989 and 2015) is marked with the southern yellow circle in d), a detailed morphological map of the study area. Cosmogenic samples were collected along the crest line close to the excavation site. e) Overview location map.

Table 2
Summary of luminescence data with the applied protocol (Method), the numbers of replicate measurements/aliquots passing the rejection criteria (n), concentration of dose rate relevant elements (K, Th, U), average dose rate, observed overdispersion (od.), equivalent dose calculated using the Central Age Model (D_e-CAM), and resulting age.

Sample	Method	n	K	Th	U	Dose rate	od.	D_e-CAM	Age
			(%)	(ppm)	(ppm)	(Gy ka^{-1})	(%)	(Gy)	(ka)
STNF 1F	IRSL	36/32	2.12 ± 0.15	4.6 ± 0.3	1.20 ± 0.30	3.11 ± 0.15	21.0	175.11 ± 6.61	56.2 ± 3.8
STNF 1F	IR-50/150	34/31	2.12 ± 0.15	4.6 ± 0.3	1.20 ± 0.30	3.11 ± 0.15	21.3	168.22 ± 6.52	54.1 ± 3.6
STNF 1F	IR-50/225	41/40	2.12 ± 0.15	4.6 ± 0.3	1.20 ± 0.30	3.11 ± 0.15	22.3	164.57 ± 5.89	52.9 ± 3.4
STNF 1F	pIR-150	34/31	2.12 ± 0.15	4.6 ± 0.3	1.20 ± 0.30	3.11 ± 0.15	24.2	164.67 ± 7.25	52.9 ± 3.7
STNF 1F	pIR-225	41/41	2.12 ± 0.15	4.6 ± 0.3	1.20 ± 0.30	3.11 ± 0.15	22.2	194.16 ± 6.84	62.4 ± 4.2
STNF 2F	IRSL	35/32	2.12 ± 0.15	4.6 ± 0.3	1.20 ± 0.30	3.11 ± 0.15	18.6	173.68 ± 5.84	55.8 ± 3.6
STNF 2F	IR-50/150	32/32	2.12 ± 0.15	4.6 ± 0.3	1.20 ± 0.30	3.11 ± 0.15	22.2	168.71 ± 6.69	54.2 ± 3.7
STNF 2F	IR-50/225	45/42	2.12 ± 0.15	4.6 ± 0.3	1.20 ± 0.30	3.11 ± 0.15	24.8	141.20 ± 5.46	45.4 ± 3.0
STNF 2F	pIR-150	32/27	2.12 ± 0.15	4.6 ± 0.3	1.20 ± 0.30	3.11 ± 0.15	27.6	172.87 ± 9.29	55.6 ± 4.3
STNF 2F	pIR-225	45/42	2.12 ± 0.15	4.6 ± 0.3	1.20 ± 0.30	3.11 ± 0.15	24.6	168.96 ± 6.49	54.3 ± 3.6
STNF 3F	IRSL	36/31	2.24 ± 0.17	5.0 ± 0.3	1.24 ± 0.20	3.25 ± 0.17	20.7	183.89 ± 6.97	56.6 ± 3.7
STNF 3F	IR-50/150	33/32	2.24 ± 0.17	5.0 ± 0.3	1.24 ± 0.20	3.25 ± 0.17	20.1	180.68 ± 6.50	55.5 ± 3.6
STNF 3F	IR-50/225	45/39	2.24 ± 0.17	5.0 ± 0.3	1.24 ± 0.20	3.25 ± 0.17	17.2	174.92 ± 4.92	53.8 ± 3.2
STNF 3F	pIR-150	33/31	2.24 ± 0.17	5.0 ± 0.3	1.24 ± 0.20	3.25 ± 0.17	21.9	191.08 ± 7.67	58.8 ± 4.0
STNF 3F	pIR-225	45/42	2.24 ± 0.17	5.0 ± 0.3	1.24 ± 0.20	3.25 ± 0.17	16.2	212.66 ± 5.74	65.4 ± 4.1

4.2. Luminescence dating

The results of luminescence dating are summarised in Table 2. Altogether the derived ages are very consistent, despite three exceptions. Two pIR-225 ages are about 10 ka older than the majority of the samples and this is interpreted to likely represent partial bleaching that, however, is not very prominently expressed in the dose distributions. One IR-50/225 age is about 10 ka lower, caused by three individual D_e values of around 70 Gy at the lower edge of the distribution. Considering the results of the storage experiments and the overall consistency of the derived ages, no fading correct was carried out. Using the entire data set delivers a weighted mean age and standard deviation of 54.9 ± 4.5 ka. If the three apparent outliers are removed, the weighted mean is 54.9 ± 1.7 ka.

4.3. Cosmogenic dating

The results of cosmogenic dating are summarised in Tables 3 and 4. Seven of the ten dates cluster in the interval 27–32 ka. Only one date, of 52.5 ka on the eastern moraine, is a clear outlier. We have rejected this date because it most likely represents prior exposure, and transport during the Late Weichselian of a boulder from the "old" felsenmeer at the summit area of Mt Nipfjället. We regard the western and eastern moraine segments as one feature, reflecting one climatic event, and have therefore calculated the means and medians, 29.4 ka and 29.8 ka respectively, of the nine accepted samples. We use the median age of 29.8 ka as the best measure of the accumulated exposure since the formation of the ridge and use this number in the discussion. The good clustering of dates is a strong indication that very little, if any, spatial rearrangement of boulders has occurred since formation of the moraine.

Table 3
Sample analytical data.

Sample ID	^{9}Be Spike (μg)	Total Qtz (g)	Total Al (μg)	Al cathode	Be cathode	^{10}Be/^{9}Be[b] (x10^{-15})	^{26}AL/^{27}Al[c] (x10^{-15})	^{26}Al/^{10}Be	^{10}Be (x10^{5} atom/g)	^{26}Al (x10^{5} atom/g)
NIP-10[a]	568	28.971	2152 ± 43	a0507	b0893	301 ± 7	1595 ± 100	6.80 ± 0.48	38.89 ± 1.25	264.43 ± 16.58
NIP-2A	237	22.469			b10245	435 ± 11			30.36 ± 0.86	
NIP-2B	237	21.031			b10246	765 ± 16			57.37 ± 1.46	
NIP-2C	238	22.146			b10247	416 ± 9			29.61 ± 0.78	
STNF-1	238	19.025			b10250	437 ± 8			36.13 ± 0.82	
STNF-2	237	24.519			b10251	550 ± 13			35.33 ± 1.01	
STNF-3	238	36.668			b10252	797 ± 20			34.38 ± 0.98	
STNF-4	238	18.727			b10253	392 ± 10			32.97 ± 0.95	
STNF-5	238	18.996			b10255	374 ± 9			30.93 ± 0.89	
STNF-6	238	19.456			b10256	300 ± 7			24.15 ± 0.67	

Uncertainties (±1s) include all known sources of analytical error.
[a] Samples processed at RSES and measured at ANSTO in 2001.
[b] Normalised to the '07KNSTD' standardization of Nishiizumi et al. (2007).
[c] Normalised to the 'KNSTD' standardization of Nishiizumi et al. (2007). No procedural blank correction because no ^{26}Al was detected.

Table 4
Sample locations and exposure ages.

Sample ID	Latitude (degrees N)	Longitude (degrees E)	Elevation (m)	Sample thickness (cm)	Shielding factor	Global Production Rate		Scandinavian Production Rate	
						^{10}Be Lm Age (ka)	^{26}Al Lm Age (ka)	^{10}Be Lm Age (ka)	^{26}Al Lm Age (ka)
NIP-10	61.9480	12.8500	1004	7	0.9998	38.6 ± 3.8 (1.2)	39.1 ± 4.5 (2.4)	36.4 ± 1.8 (1.2)	36.9 ± 2.7 (2.4)
NIP-2A	61.9562	12.8525	1000	2	2.6	29.3 ± 2.9 (0.8)		27.6 ± 1.3 (0.8)	
NIP-2B	61.9562	12.8525	1000	2	2.6	55.7 ± 5.4 (1.4)		52.5 ± 2.3 (1.4)	
NIP-2C	61.9562	12.8525	1000	2	2.6	28.6 ± 2.8 (0.7)		26.9 ± 1.2 (0.7)	
STNF-1	61.9489	12.8478	1008	1	0.9998	34.1 ± 3.3 (0.8)		32.1 ± 1.4 (0.7)	
STNF-2	61.9489	12.8477	1008	3	0.9998	33.7 ± 3.3 (0.9)		31.7 ± 1.5 (0.9)	
STNF-3	61.9489	12.8477	1008	3	0.9998	32.9 ± 3.2 (0.9)		31 ± 1.4 (0.9)	
STNF-4	61.9491	12.8474	1008	4	0.9998	31.7 ± 3.1 (0.9)		29.8 ± 1.4 (0.9)	
STNF-5	61.9490	12.8474	1008	2	0.9998	29.4 ± 2.9 (0.8)		27.6 ± 1.3 (0.8)	
STNF-6	61.9487	12.8481	1008	4	0.9998	23.2 ± 2.3 (0.6)		21.8 ± 1 (0.6)	

[a] Calculated using version 2.3 of the online exposure age calculators formerly known as the CRONUS-Earth online exposure age calculators (Balco et al., 2008) using the Lm scaling method with the default Global Production rates and with the Scandinavian Production Rate derived from the ICE-D database. Internal uncertainties (±1s, shown in parentheses) reflect analytical uncertainties on sample processing and ^{10}Be measurements. External uncertainties (±1s) incorporate in addition uncertainties in the calibration and scaling procedure. Calculated exposure ages assume a post-exposure erosion rate (e) of 0 mm ka^{-1}. Calculation of ages for e = 1 mm ka^{-1} increases the above ages by 1% per 10ka.

5. Discussion

The sand lens in which luminescence dates were measured is an integral part of the moraine ridge and must have been deposited during its formation (Fig. 12:1). The parental material is inferred to be sub- and supraglacial till washed and sorted over short distances in a subaerial setting (Fig. 12:2). With the addition of new till material directly at the margin, lateral shifting of supraglacial streams, and subsequent burial, the result is isolated layers or pockets of sand (Fig. 12:3). The boulders on the ridge crest are interpreted as normal components of the till.

The moraine ridge is regarded as a true marginal moraine because of: (1) its position at the edge of a till sheet, (2) its morphology, with a proximal slope steeper than the distal slope, is typical of a marginal moraine ridge, and (3) its inner composition of mostly till, with a faint layering sloping in the distal direction.

The western moraine segment runs in a generally NNW – SSE direction. The common presence in the till of Frönberg gneiss suggests that the till was transported tens of km from the northwest sector before reaching the moraine. With such a flow configuration ice would have to flow around the western edge of Mt Nipfjället, rather than across the high plateau. If these inferences are correct, the small valley probably constituted a local ablation area, into which the ice flow was restricted. The moraine cannot with certainty be traced as a single ridge into this valley, but the presence of morphologically less ordered heaps of material on the valley floor indicates that an ice tongue extended into it from the SW, with ice surface elevation some tens of meters lower than the ridge crest at the excavation site (see Fig. 13 for a tentative reconstruction). We have been guided by the ice surface morphology at present day nunataks in Antarctica and elsewhere, where depressions on the lee side (in relation to ice flow) often form local ablation areas with ice surface elevations significantly lower than lateral settings.

The western and eastern moraine segments are not in physical contact but we reason that their similarity in morphology and elevation, and the observation that both mark the upslope limit of the till sheet, are strong indications that they represent the same event, a climatic standstill of the ice margin.

We note that ice supply to the eastern moraine is unlikely to have come around the western edge of Nipfjället, but is instead likely to have followed a more complicated route east of the main summit of Nipfjället. It is likely but cannot be strictly demonstrated that the single grossly deviating exposure age for the eastern moraine (52.5 ± 2.3 ka) is related to mobilization of a boulder from preserved old boulder fields known to exist at the summit areas of Nipfjället.

The extreme degree of morphological preservation of this small-scale moraine is a strong indication that the Last Weichselian Ice Sheet did not erode the site, with sustained cold-base conditions being the only realistic explanation.

The assumption we employ in linking datings to the landform, and which also allows us to make inferences about ice sheet extent is that the moraine is a true marginal feature. At the time of formation it separated ice-free and ice-covered terrain. The two materials that were dated, sand within the moraine ridge and boulders on top, were likely deposited within a time span that is short compared to the time that has elapsed since ridge formation.

The use of a dating method (luminescence) should give a true age for the landform. The use of an exposure duration method (cosmogenic nuclides) applied to the same landform, allows elapsed ice-free time since its formation to be measured. A third important piece of information, the duration of ice cover, should be the difference between the two. In the following discussion we adopt a mean age of ca. 55 ka for the luminescence samples and infer that this is also the age of the landform. The cosmogenic samples indicate approximately 30 ka of subaerial exposure after the formation of the moraine. Final deglaciation at the site occurred around 10 ka (Stroeven et al., 2016). For the Idre area, reconstruction by Stroeven et al. (2016) is not based on any local dating, but rather varve dating of localities hundreds of kilometres away and extrapolation from accurately known deglaciation speeds in central Sweden. We estimate the uncertainty for this age assignment to be on the order of ca. 200 years at Idre. This is a small uncertainty compared to the uncertainties related to the luminescence and ^{10}Be dating at the site. For Fig. 15, we consider Holocene exposure of the site to have lasted some 10 ka. An accumulated ice-free time of ca. 20 ka during one or more interstadials is thus indicated.

Because of the nature of the data, involving two different dating

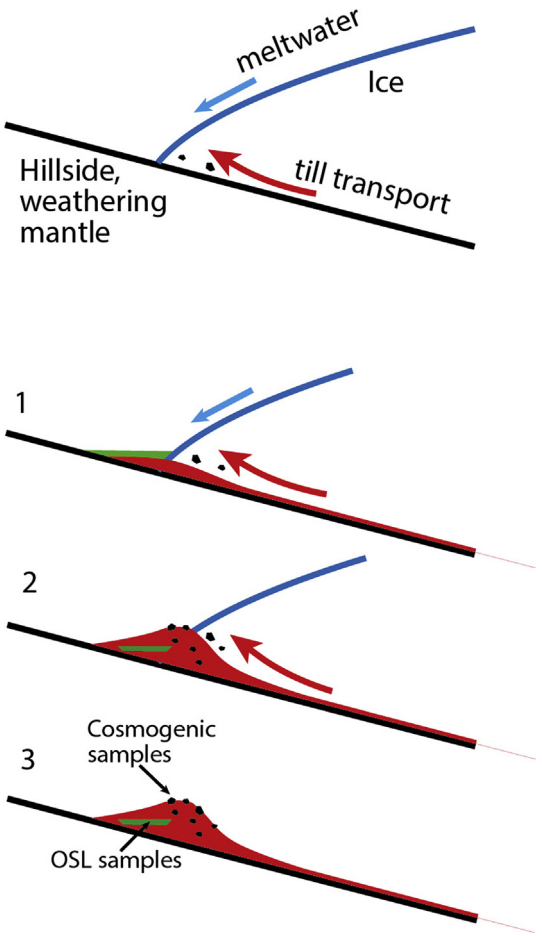

Fig. 12. Scheme for the inferred sequence of sedimentation events during the formation of the ridge. 1) Debris transported by meltwater is sorted and deposited into planar sand deposits. Simultaneously till is deposited at the ice margin. Finally, the ridge is mainly a till feature. 2) Boulders are an integral part of the till. 3) The ridge today retains much of its inferred original shape. The age of surficial boulder emplacement can be no older than the emplacement and optical exposure of sand lenses.

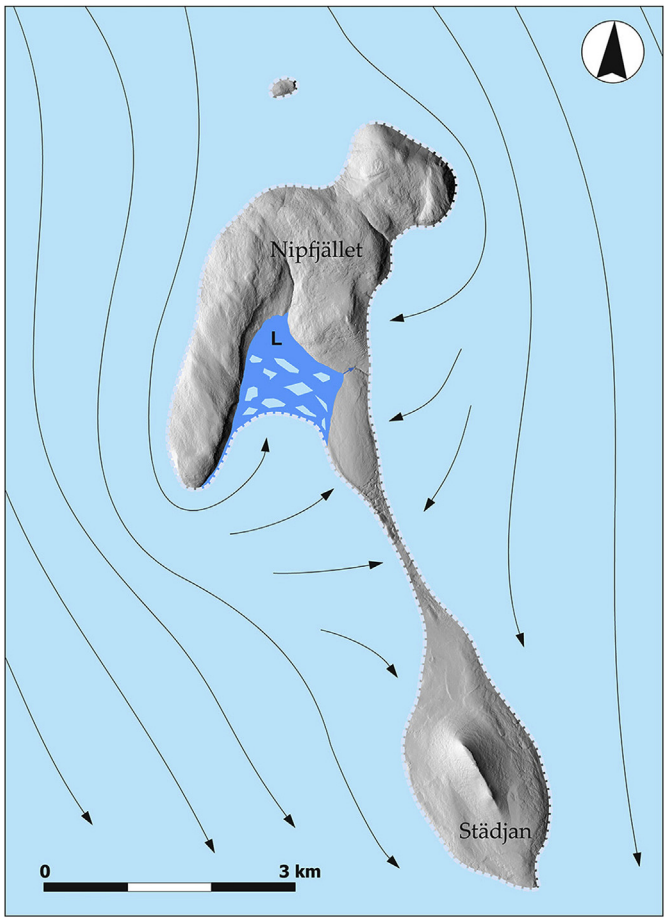

Fig. 13. The inferred ice flow pattern at the time of moraine ridge formation. A general flow direction from the NNW is indicated by patches of faint fluting in the surrounding area (Borgström 1989, 2017 (Map 3 Stadjan-Nipfjallet.jpg)). L symbolizes a glacial lake.

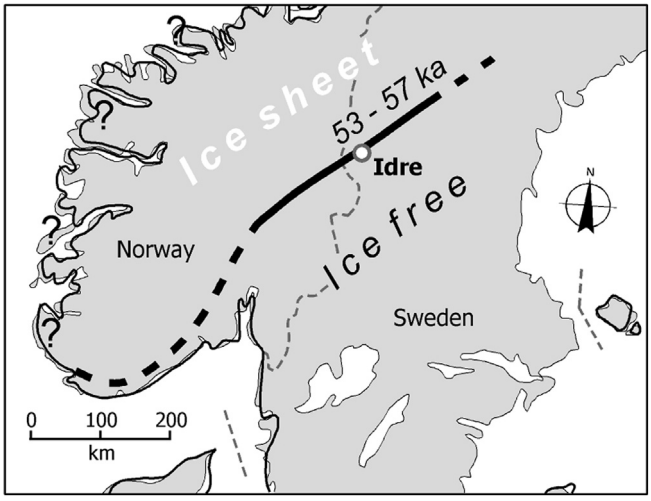

Fig. 14. The luminescence data from the Idre moraine, the configuration of the moraine, and the inferred transport direction of erratics indicates the presence of a limited west-centred Norwegian-Swedish ice sheet at 53–57 ka.

methods, and well-defined error margins only covering analytical uncertainties for the luminescence data but not geological uncertainties, a strict analysis of errors is difficult to perform. We acknowledge significant uncertainty regarding precise ages and durations. We reason that luminescence and cosmogenic dating uncertainties are additive for determining when the Late Weichselian ice sheet expanded over the site, because the starting time for exposure (around 55 ka) carries its own uncertainty. We regard the data to indicate ridge formation at 54.9 ± 1.7 ka, ice-free exposure of the moraine ridge for around 30 ka and duration of interstadial conditions around 20 ka. A straightforward interpretation is that a single ice-free period started in the interval 57-53 ka and lasted until 37-33 ka, with some additional and not quantified uncertainty for the latter figure.

Ice cover at Idre is compatible with a small west-centred ice sheet over Norway, but also compatible with a Fennoscandian Ice Sheet with a large easterly extent. Evidence for a margin located at Idre, and hence *ice-free conditions* offers a much more restricted set of possibilities. The site offers direct evidence for transport of material from the NW sector, and the moraine by nature pinpoints a specific location of the ice margin. There are thus good indications that a Norway-centred ice sheet existed at the time of ridge formation (Fig. 14). Small-sized mountain-centred ice sheets have been discussed and reconstructed by many authors (Ljungner, 1949; Porter, 1989; Kleman, 1992). Such an ice configuration is climatologically plausible because of the presence of a linear mountain belt in a setting with a strong west-east mass balance gradient. In contrast, it appears climatologically implausible to have ice-free conditions at Idre concurrently with ice cover east of this location, and no evidence for such a configuration has been reported.

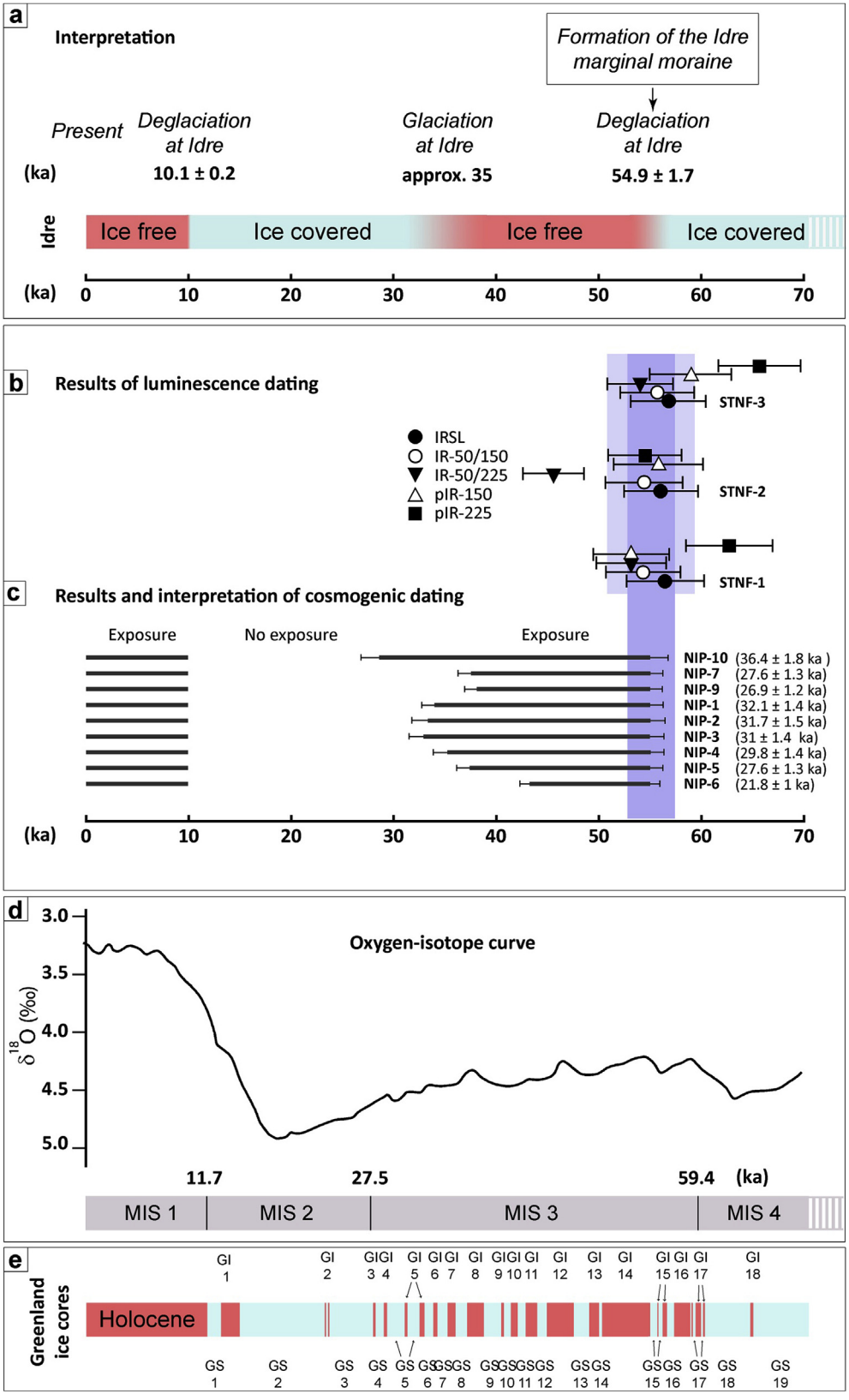

Fig. 15. (a) Interpretation of stadial/interstadial events at Idre.
(b) Luminescence dates from the section in the Idre moraine. The bar indicates one and two standard deviations, centred on the mean luminescence age of 54.9 ± 1.7 ka. This age clearly falls into the period of lowering of global ice volume (d), likely representing interstadial conditions in Scandinavia.
(c) Cosmogenic (^{Be}10) dates from the Idre moraine. The dates, which are exposure durations rather than absolute dates, are plotted with the mean luminescence age of 54.9 ka as the baseline. Around 10 ka of exposure is accounted for by Holocene exposure. The remainder of the exposure for each sample is plotted as interstadial exposure.
(d) Benthic oxygen-isotope curve largely reflecting global ice volume (Lisiecki and Stern, 2016). Global ice volume is a geographically integrated and therefore smoothed and dampened response to more rapid climatic shifts (e).
(e) Event stratigraphy based on three synchronized Greenland ice-core records (Rasmussen et al., 2014).

Our data has bearing on the speed of ice sheet build-up after the MIS 3 interstadial(s). Accepting an LGM age of around 21 ka, the build-up from no ice or a very small ice volume occurred in 10–18 ka. This can be compared to the final shrinkage and full deglaciation being achieved in around 11 ka. We note that the timing of the LGM may be less easy to define than previously thought and can well be a few thousand years older than the often used 21 ka (Hughes et al., 2016), which would give a correspondingly shorter build-up time.

The Late Weichselian Ice Sheet appears to have been short-lived with rapid expansion and retreat phases. The presence of centrally located

frozen-bed zones have been suggested many times previously (Sollid and Sørbel, 1988; Lagerbäck, 1988; Kleman and Borgström, 1994; Hättestrand, 1997; Kleman and Hättestrand, 1999). The preservation of delicate landforms reported here is very difficult to explain without invoking an at least partially frozen bed for the duration of the LW ice cover.

The age assignment of 55 ka from luminescence dating coincides with the onset of the first long and warm MIS interstadial (GI 14, Fig. 15) but we note that the dating uncertainty and the fact that ice volume variations are an integrated response (Fig. 15c) to the total effect of many short-lived climatic events (Fig. 15d) makes such detailed correlation dubious. However, from Fig. 15 it appears likely that the Idre moraine formed during an early part of the long interstadial MIS 3 complex. By itself it implies the existence of a Norwegian ice sheet remnant at that time. As an end moraine of this type by nature reflects a standstill of the ice margin, our conclusion is that the moraine formed as a response to a climatic deterioration during the generally warm climate in the early part of MIS 3. The data cannot illuminate whether Scandinavia became entirely ice-free during MIS 3, just that any ice sheet remnant must have been small and located northwest of Idre. We estimate that the maximum sea-level contribution of the Scandinavian ice sheet at around 55 ka was less than 1m.

6. Conclusions

An ice-marginal moraine from a Norway-centred pre-Late Weichselian ice sheet was luminescence dated and found to have formed approximately 55 ka, during the early warm part of MIS 3. Cosmogenic dating of rooted boulders on top of the moraine indicate that it has received about 30 ka of subaerial exposure since formation. Only 10 ka of exposure can be accounted for by the Holocene, leading to the conclusion that the moraine was exposed for around 20 ka during a MIS 3 interstadial. Co-analysis of cosmogenic and luminescence ages suggest that the interstadial at Idre ended by expansion of the Scandinavian Ice Sheet over the site at around 35 ka. The degree of preservation of the moraine indicates sustained cold-based conditions at the site during the Late Weichselian. Our results show that the Late Wecihselian ice sheet was more dynamic than previously thought, with advance speeds up to the LGM rivalling the pace of deglaciation in central Sweden.

Declaration of competing interest

There are no conflicts of interest.

Acknowledgment

This study was funded by grants from the Swedish Research council to Johan Kleman.

References

Auclair, M., Lamothe, M., Huot, S., 2003. Measurement of anomalous fading for feldspar IRSL using SAR. Nucl. Sci. Technol. 37, 487–492.
Aylsworth, J.M., Shilts, W., 1989. Bedforms of the keewatin ice sheet, Canada. Sediment. Geol. 62, 407–428.
Balco, G., Stone, J.O., Lifton, N.A., 2008. A complete and easily accessible means of calculating surface exposure ages or erosion rates from Be-10 and Al-26 measurements. Quat. Geochronol. 3, 174–195.
Borchers, B., Marrero, S., Balco, G., Caffee, M., Goehring, B., Lifton, N., Nishiizumi, K., Phillips, F., Schaefer, J., Stone, J., 2016. Geological calibration of spallation production rates in the CRONUS-Earth project. Quat. Geochronol. 31, 188–198.
Borgström, I., 1989. Terrängformerna och den glaciala utvecklingen i de södra fjällen, vol. 234. Department of Physical Geography, University of Stockholm, Meddelande, p. 133p.
Borgström, I., 2017. Geomorphology and Exposure Datings in West-Central Sweden. Bolin Centre Database. Bolin Centre for Climate Research, Stockholm University, Sweden. http://bolin.su.se/data/Borgstrom-2017.
Buylaert, J.P., Jain, M., Murray, A.S., Thomsen, K.J., Thiel, C., Sohbati, R., 2012. A robust feldspar luminescence dating method for Middle and Late Pleistocene sediments. Boreas 41, 435–451.
Degering, D., Degering, A., 2020. Change is the only constant - time-dependent dose rates in luminescence dating. Quat. Geochronol. 58, 101074 (in press).
Delin, H., Thelander, T., 2006. Kartområdena 16C Idre, 16D Lofsdalen NV och SV samt 17C Funäsdalen SV och SO. In: Delin (Ed.), Berggrundsgeologisk Undersökning, Rapporter Och Meddelanden 126. SGU, pp. 146–160.
Galbraith, R.F., Roberts, R.G., Laslett, G.M., Yoshida, H., Olley, J.M., 2007. Optical dating of single and multiple grains of quartz from Jinmium roch shelter, Northern Australia: Part I, experimental design and statistical models. Archeometry 41 (2), 339–364.
Helmens, K.F., Risberg, J., Jansson, K.N., Weckström, J., Berntsson, A., Kaislahti Tillman, P., Johansson, P.W., Wastegård, S., 2009. Early MIS 3 glacial lake evolution, ice-marginal retreat pattern and climate at Sokli (northeastern Fennoscandia). Quat. Sci. Rev. 28, 1880–1894.
Hughes, A.L.C., Gyllencreutz, R., Lohne, Ø.S., Mangerud, J., Svendsen, J.I., 2016. The last Eurasian ice sheets – a chronological database and time-slice reconstruction, DATED-1. Boreas 45, 1–45.
Huntley, D.J., Baril, M.R., 1997. The K content of the K-feldspars being measured in optical dating or in thermoluminescence dating. Ancient TL 15 (1), 11–13.
Hättestrand, C., 1997. Ribbed moraines in Sweden—distribution pattern and palaeoglaciological implications. Sediment. Geol. 111, 41–56.
Hättestrand, M., Robertsson, A.-M., 2010. Weichselian interstadials at Ripiharju, northern Sweden: interpretations from fossil and modern pollen records. Boreas 39, 296–311.
Kleman, J., 1988. Linear till ridges in the southern Norwegian— Swedish mountains: evidence for a subglacial origin. Geogr. Ann. 70A, 35—45.
Kleman, J., Borgström, I., 1990. The Boulder fields of Mt. Fulufjället, west-central Sweden - Late Weichselian boulder blankets and interstadial periglacial phenomena. Geogr. Ann. 72A, 63–78.
Kleman, J., Borgström, I., 1994. Glacial landforms indicative of a partly frozen bed. J. Glaciol. 135, 255–264.
Kleman, J., Stroeven, A.P., 1997. Preglacial surface remnants and Quaternary glacial regimes in northwestern Sweden. Geomorphology 19, 35–54.
Kleman, J., 1992. The palimpsest glacial landscape in northwestern Sweden — Late Weichselian deglaciation landforms and traces of older west-centered ice sheets. Geogr. Ann. 74A, 305–325.
Kleman, J., Hättestrand, C., 1999. Frozen-bed Fennoscandian and Laurentide ice sheets during the last glacial maximum. Nature 402, 63–66.
Kleman, J., Hättestrand, C., Borgström, Stroeven, A.P., 1997. Fennoscandian paleoglaciology reconstructed using a glacial geological inversion model. J. Glaciol. 43, 283–299.
Kohl, C.P., Nishiizumi, K., 1992. Chemical isolation of quartz for measurement of in-situ-produced cosmogenic nuclides. Geochem. Cosmochim. Acta 56, 3583–3587.
Lagerbäck, R., 1988. Periglacial phenomena in the wooded areas of Northern Sweden—relicts from the Tärendö interstadial. Boreas 17, 487–499.
Lagerbäck, R., Robertsson, A.-M., 1988. Kettle holes – stratigraphical archives for Weichselian geology and paleoenvironment. Boreas 17, 439–468.
Lal, D., 1991. Cosmic ray labeling of erosion surfaces: in situ nuclide production rates and erosion models. Earth Planet Sci. Lett. 104, 424–439.
Lisiecki, L.E., Stern, J.V., 2016. Regional and global benthic $\delta^{18}O$ stacks for the last glacial cycle. Paleoceanogr. Paleoclimatol. 31 (10) https://doi.org/10.1002/2016PA003002.
Lowick, S.E., Trauerstein, M., Preusser, F., 2012. Testing the application of post IR-IRSL dating to fine grain waterlain sediments. Quat. Geochronol. 8, 33–40.
Ljungner, E., 1949. East–west balance of the quaternary ice caps in Patagonia and Scandinavia. Bull. Geol. Inst. Univ. Upps 33, 11–96.
Lundqvist, J., Miller, U., 1992. Weichselian stratigraphy and glaciations in the Tåsjö-Hoting area. Central Sweden. Sveriges Geologiska Undersökning C 826, 1–35.
Mangerud, J., 1991a. The last ice age in Scandinavia. In: Andersen, B.G., Königsson, L.-K. (Eds.), Late Quarernary Stratigraphy in the Nordic Countries 150,000-15,000 B.P., pp. 15–30. Striae 34.
Mangerud, J., 1991b. The Scandinavian ice sheet through the last interglacial/glacial cycle. In: Klimageschichtiche Probleme der letzen 130,000 Jahre. B. Frenzel, pp. 307–330.
Mannerfelt, C.M., 1938. Das hervorschmelzen des Städjanberges aus dem absterbenden Inlandeis. Geografiska Föreningens Förhandlingar 60, 405–422.
Mannerfelt, C.M., 1945. Några glacialmorfologiska formelement och deras vittnesbörd om landisens avsmältning i svensk och norsk fjällterräng. Geogr. Ann. 27, 239.
Murray, A.S., Wintle, A.G., 2000. Luminescence dating of quartz using an improved single-aliquot regenerative-dose protocol. Radiat. Meas. 32, 57–73.
Nishiizumi, K., Imamura, M., Caffee, M.W., Southon, J.R., Finkel, R.C., McAninch, J., 2007. Absolute calibration of 10 Be AMS standards. Nucl. Instrum. Methods Phys. Res. B 258, 403–413.
Porter, S.C., 1989. Some geological implications of average quaternary glacial conditions. Quat. Res. 32, 245–261.
Prescott, J.R., Hutton, J., 1994. Cosmic ray contributions to dose rates for luminescence and ESR dating: large depths and long-term time variations. Radiat. Meas. 23, 497–500.
Preusser, F., Kasper, H.U., 2001. Comparison of dose rate determination using high-resolution gamma spectrometry and inductively coupled plasma - mass spectrometry. Ancient TL 19, 19–23.
Rasmussen, S.O., Bigler, M., Blockley, S.P., Blunier, T., Buchardt, S.L., Clausen, H.B., Cvijanovic, I., Dahl-Jensen, D., Johnsen, S.J., Fischer, H., Gkinis, V., Guillevic, M., Hoek, W.Z., Lowe, J.J., Pedro, J.B., Popp, T., Seierstad, I.K., Steffensen, J.P., Svensson, A.M., Vallelonga, P., Vinther, B.M., Walker, M.J.C., Wheatley, J.J., Winstrup, M., 2014. A stratigraphic framework for abrupt climatic changes during the Last Glacial period based on three synchronized Greenland ice-core records: refining and extending the INTIMATE event stratigraphy. Quat. Sci. Rev. 106, 14–28.

Reimann, T., Tsukamoto, S., Harff, J., Osadczuk, K., Frechen, M., 2011. Reconstruction of Holocene coastal foredune progradation using luminescence dating – an example from the Świna barrier (southern Baltic Sea, NW Poland). Geomorphology 132, 1–16.
Richter, D., Richter, A., Dornich, K., 2013. Lexsyg - a new system for luminescence research. Geochronometria 40 (4), 220–228.
Sollid, J.L., Sørbel, L., 1988. Influence of temperature conditions in formation of end moraines in Fennoscandia and Svalbard. Boreas 17, 553–558.
Stone, J.O., 2000. Air pressure and cosmogenic isotope production. J. Geophys. Res.: Solid Earth 105, 23753–23759.
Stroeven, A.P., Hättestrand, C., Kleman, J., Heyman, J., Fabel, C., Fredin, C., Goodfellow, B.W., Harbor, J.M., Jansen, J.D., Olsen, L., Caffee, M.W., Fink, D., Lundqvist, J., Rosqvist, G., Strömberg, B., Jansson, K., 2016. Deglaciation of Fennoscandia. Quat. Sci. Rev. 147, 91–121.
Sugden, D.E., Watts, S.H., 1977. Tors, felsenmeer and glaciation in northern Cumberland peninsula, Baffin Island. Can. J. Earth Sci. 14, 2817–2823.
Ukkonen, P., Aaris-Sörensen, K., Arppe, L., Clark, P.U., Daugnora, L., Lister, A.M., Lougas, L., Seppä, H., Sommer, R.S., Stuart, A.J., Wojtal, P., Zupins, I., 2011. Wooly mammoth (Mammthus primigenius Blum.) and its environment in modern Europé during the last glaciation. Quat. Sci. Rev. 30, 693–712.
Wallinga, J., Bos, A.J.J., Dorenbos, P., Murray, A.S., Schokker, J., 2007. A test case for anomalous fading correction in IRSL dating. Quat. Geochronol. 2, 216–221.
Wintle, A.G., Murray, A.S., 2006. A review of quartz optically stimulated luminescence characteristics and their relevance in single-aliquot regeneration dating protocols. Radiat. Meas. 41 (4), 369–391.
Wohlfarth, B., 2010. Ice-free conditions in Sweden during marine oxygen isotope stage 3? Boreas 39, 377–398.
Young, N.E., Schaefer, J.M., Briner, J.P., Goehring, B.M., 2013. A ^{10}Be production-rate calibration for the Arctic. J. Quat. Sci. 28, 515–526.